Distribution Agreement

In presenting this thesis as a partial fulfillment of the requirements for a degree from Emory University, I hereby grant to Emory University and its agents the non-exclusive license to archive, make accessible, and display my thesis in whole or in part in all forms of media, now or hereafter now, including display on the World Wide Web. I understand that I may select some access restrictions as part of the online submission of this thesis. I retain all ownership rights to the copyright of the thesis. I also retain the right to use in future works (such as articles or books) all or part of this thesis.

Kyle Kairys March 28, 2022

Quantum Energy Diffusion in Polaritonic Wires

By

Kyle Kairys

Raphael Ribeiro

Adviser

Chemistry

Francesco Evangelista

Committee Member

Brenda Harmon

Committee Member

2022

Quantum Energy Diffusion in Polaritonic Wires

By

Kyle Kairys

Dr. Raphael Ribeiro

Adviser

An abstract of
a thesis submitted to the Faculty of Emory College of Arts and Sciences
of Emory University in partial fulfillment
of the requirements of the degree of
Bachelor of Science with Honors

Chemistry

2022

Abstract

Quantum Energy Diffusion in Polaritonic Wires

By Kyle Kairys

The worsening climate crisis has placed increased emphasis on the development of novel modes of sustainable energy generation and transport. A major inhibition to this process is the fast and efficient transport of energy. Quantum energetic phenomena of organic polaritons in optical microcavities have demonstrated significant potential to revolutionize modes of energy transfer. In this work, the definition of short-time, spatial diffusion was investigated for these systems and their coherent energy transfer dynamics. This investigation implemented a microscopically detailed computational photonic wire model that evaluates spacetime resolved energy diffusion. All simulations conducted employed the use of an initial state described by a molecular excited-state Gaussian wavepacket. This study modulated alterations to the internal system parameters of light-matter coupling strength, total system size, and variance of molecular excited-state energy fluctuations. This was done to effectively elucidate their impact on the intermolecular energy transport of the polaritonic system. In the absence of fluctuations in the molecular excited-state energies, ballistic intermolecular energy transport dynamics were observed within the femtosecond timescale; this observation however was not upheld for systems with energetic disorder. Diffusion constants were simulated for systems experiencing strong and weak energetic disorder. Within the strong disorder case, the introduction of disorder above a specific critical value of the light-matter interaction, resulted in the excited states of the system to become highly localized and trap the energy. This observation was upheld for a 20-picosecond time scale. In the case of weak disorder, relative to the light-matter interaction strength, diffusion constants increase as the disorder of the system is decreased. Through evaluation of molecular density, it was determined that a smaller system density results in increased transport properties because the single molecular dipole moments scale with intermolecular distances. It was also determined that for sufficiently small intermolecular distances, simulated diffusion constants were seemingly independent of system size, however with larger intermolecular distances there appeared to be a significant transport dependence on system size. This investigation has evaluated novel properties of quantum intermolecular energy transport in photonic wires, and it has determined that such behavior is relatively controllable through the characteristics of polaritonic devices. This demonstrates significant potential for the control of molecular material dynamics in optical cavities.

Quantum Energy Diffusion in Polaritonic Wires

By

Kyle Kairys

Dr. Raphael Ribeiro

A thesis submitted to the Faculty of Emory College of Arts and Sciences
of Emory University in partial fulfillment
of the requirements of the degree of
Bachelor of Science with Honors

Chemistry

2022

Acknowledgement

I would like to thank Dr. Ribeiro for all of his hard work and guidance in facilitating my work and introduction into the field of computational quantum optics. Additionally, I would like to thank both committee members, Professor Brenda Harmon and Dr. Francesco Evangelista, for their support and mentoring throughout my undergraduate career. Finally, I would like to acknowledge the support and feedback provided by the Ribeiro lab and all of its members.

Table of Contents

1. General Background

1.1 Energy Transport

As technologies advance and climate conditions worsen, novel innovations seek to propel the fields of energy generation and efficient transport forward. [1,2] Although seemingly innumerable, applications of enhanced energy transport stand to revolutionize not only environmental innovations, but also various other spectroscopic devices such as spectrometers and satellites. [3,4] This incredible dependence of technological innovation on fairly fundamental principles regarding energy transfer has fostered resolve to advance this field. A major challenge lies for example in limitations to solar energy conversion into electricity with organic materials. Low efficiency excited-state energy transport into charge-transfer regions of a device precludes efficient conversion of sunlight into usable electric currents. [5-7] This, among many other fields of interest, has driven vast explorations into the dynamics and underlying processes that describe transport phenomena. [8,9]

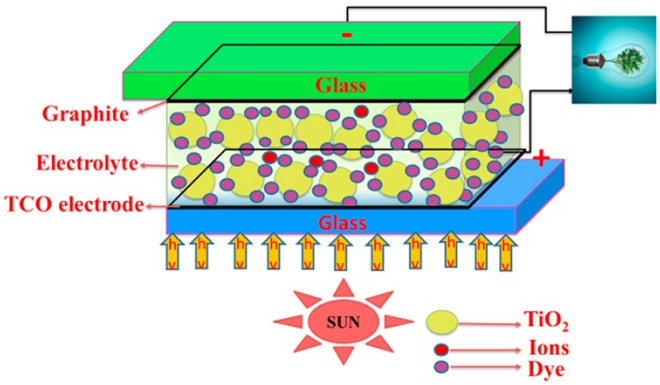

Figure 1. General schematic for organic, TiO_2, solar cell. [10]

Through fundamental understandings of energy transfer, it is evident that the advancement of these dynamics lies in the interactions between light and matter. Both these photonic and molecular regimes have varying degrees of energy transfer capacity and therefore differ in terms of their relative utilities. Despite their differing dynamics, there remain significant

points of intersection, between the energy transfer of light and matter, that pose large potential to advance understanding of their individual and novel properties. [11,12]

1.2 Polaritons

Polaritons are hybrid light-matter particles that are formed from the strong interaction of photons and the dipole-active transitions of molecule or other materials. [13] These quasiparticles are defined by their hybrid composition allowing them to experience both molecular and photonic characteristics. Polaritons have been observed to exist within a range of different materials, but their formation is limited to specific materials that can effectively allow energy exchange between molecules and electromagnetic fields before decay. [14] Polaritons are most widely known to be found within both highly ordered solid state materials like crystals, and within the surfaces of metal-nanomaterials. [15] Despite their apparent limitations to a solid phase, polaritons are also largely observed to be delocalized over molecular systems in the liquid and gas phases within unique devices known as optical microcavities. [16-18]

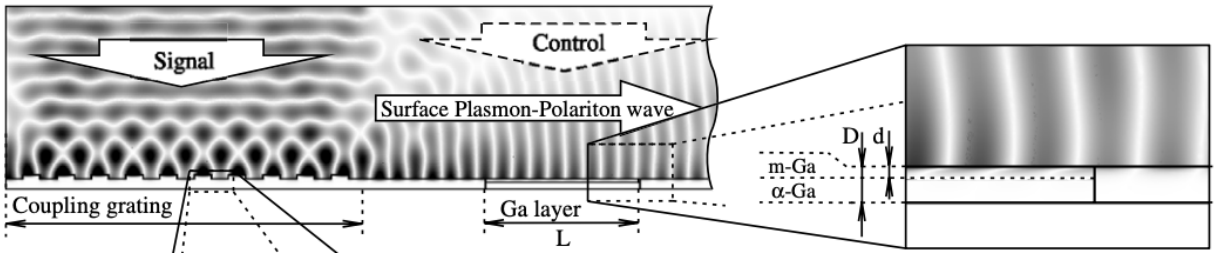

Figure 2. Gold on silica waveguide for the creation of a surface plasmon polariton, that is imaged using field mapping to show the z-component of the magnetic field. [19]

1.2.1 Optical Microcavities

Optical microcavities are devices that support polaritons under a wider range of conditions. These cavities are composed of high reflectivity mirrors, that are normally made from either highly ordered nanostructures or layered semiconductor materials, that surround a gap that is filled with target molecules and a disordered phase. These optical cavities have confined resonant photonic modes. The cavities can be designed so one more of their modes are specifically selected to be resonant with various excitations of molecular ensembles. These resonances allow for the effective formation of the cavity polariton modes. Light confinement by the mirrors makes microcavities much more efficient in the production of polaritons and allow for significant tuning of their properties.

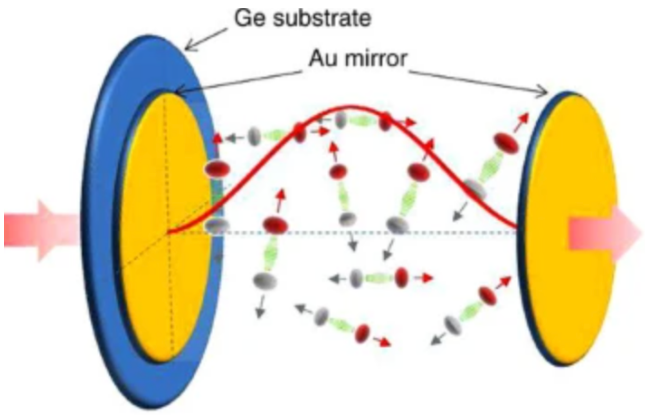

Figure 3. General optical microcavity schematic. [20]

The tuning of the properties within an optical microcavity is associated to varying factors of the cavity itself as well as the incidence of the light input into the system which can modulate the energies of the excited photonic (cavity) modes. The internal energy dynamics of an optical microcavity are dominated by three major processes: (1) the rate of energy exchange between light and matter, (2) the rate that light escapes the cavity, and (3) the rate at which the matter loses its coherent polarization (dephasing rate). [21] The system is considered to be within the

strong coupling regime when the rate of energy exchange greatly exceeds that of the rates of processes (2) and (3). [21] This results in the periodic exchange between light and matter.

Optical microcavities can differ significantly based on the type of target molecule that is used within the cavity. Various studies have investigated the utility of both inorganic and organic target molecules. [22,23] Given the interest in organic materials for new optoelectronic technologies and solar energy conversion devices, this project seeks to evaluate the impacts of utilizing organic molecules within polaritonic microcavities. Organic aggregates often have electronic transitions with intense absorption spectrum allowing them to experience strong light-matter interactions with the photons of optical microcavities, but also a much stronger interaction with phonons and a much greater heterogeneity in their transition energies. [24] Additionally, organic molecules exhibit significant dynamical changes through interaction with the polaritonic modes of an optical microcavity. They have been demonstrated to facilitate charge transport phenomena [25], as well as exhibit alterations to their Photochemistry and Photophysics, associated to spin interconversions. [21, 26]

Optical microcavities, or optical resonators as they are sometimes noted, have demonstrated significant and novel potential for chemical advancement. The unique combination of polaritonic modes within a disordered phase demonstrates compelling utility to explore many new phenomena. As Thomas et al. indicates in their work, there may be potential employing these quantum optical phenomena to control reaction dynamics. [27] Similarly, Krainova et al. explores its utility in advancing photoconductivity. [12] Finally, Coles et al. describes the immense capacity that polaritonic microcavities have for advancements in energy transfer. [28]

1.2.2 Light-Matter Coupling Strength

Within optical microcavities, the light-matter exchange rate is defined by the probability of the molecules to be excited by the cavity mode, in other words, by the light-matter coupling strength. Cavity modes with varying incidence angles have different energies which are more or less resonant with the molecular excitation of choice.

The pure molecular excitation and the pure cavity modes are coupled to form two unique bands that are denoted upper and lower Polariton or UP and LP respectively. The formation of these polaritons dominates the phenomena that occur within the coupled system. [29]

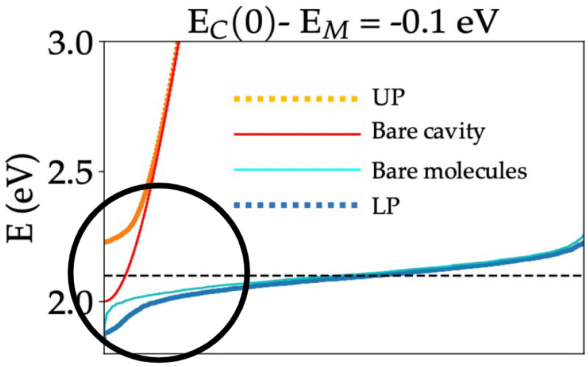

Figure 4. General polariton dispersion diagram. Demonstrates the splitting of the bare photonic and molecular systems into both UP and LP bands. Detuning for this system is -0.1eV. [17]

The energy of separation between the polariton bands as indicated in the dispersion diagram in Fig 4, is denoted Rabi Splitting or Ω_R. This number qualifies the strength of the light matter coupling within a given system. A different yet similarly important value is known as the detuning of the system. This value describes the difference between the bare molecular excitation energy of the system and the energy of the lowest energy cavity mode. The detuning is an important quantity as by changing the molecular excitation energy while maintaining the fixed

cavity (or vice versa), you can effectively increase the energetic overlap of the molecular and photonic bands.

1.3 Energetic Diffusion

The quantum delocalized nature of polaritons inherently alters many of the separate aspects of both light and matter. Individually, light and matter possess very different diffusive properties. Light typically propagates extremely fast and exhibits what is known as *ballistic* transport. This type of transport is generally associated with a linear dependence on time. Contrarily, energy in most molecular materials tends to propagate much slower and in a generally much less efficient manner. This type of diffusion is noted simply as *diffusive* behavior. The following Equations 1 and 2, respectively demonstrate the mathematical expressions for these two processes of ballistic and diffusive behavior.

$$\Delta x = vt \tag{1}$$

$$\Delta x^2 = 2Dt \tag{2}$$

Within the above Equations, 1 and 2, the delta x squared values indicate the displacement squared, the uppercase D is the diffusion constant for the specific system, and t indicates time. These expressions are used in order to characterize the energy flow in a system. The D terms from these equations are generally identified as *diffusion constants*. The generation of these terms is generally used to identify and qualify the energy transport exhibited by a given system.

Since microcavity polaritons are most explicitly identified by their delocalized light-matter dual nature, the diffusivity of energy in these systems can vary significantly depending on

the internal system parameters like initial-state, cavity matter interaction strength, etc. Although there have been various experiments which have intended to investigate this phenomenon, significant gaps in understanding energy transport remain. There is significant evidence that energetic disorder is largely impactful on these polariton modes, especially in organic cavities due to the contribution of Frenkel excitations. [36] Additionally many older computational models have sought to utilize a single cavity mode as the only contributing mode to the formation of cavity polaritons, which largely fails to represent the entire multimode system, especially when there are considerations of significant system detuning. [17,18] [31] These limited views of a still largely misunderstood phenomena established the basis for further investigation into the nature of energy diffusion in organic microcavity polaritons.

As is explained by Raj et. al. there are no accounts of spatial-temporal energy evolution throughout a cavity, in extremely small-time scales such as the sub picosecond regime. [21] Although Raj et al. has begun to evaluate some small-time scale polariton propagation dynamics there remains substantial lack of understanding of the characteristics of space-time resolved energy diffusion in polaritonic materials. This project employs computational methods to analyze spacetime-resolved energy diffusion in disordered multimode organic microcavity polaritons.

2. Computational Methods

2.1 Physical Model

2.1.2 Photonic Wire Model

The structure used to facilitate the study of these optical microcavity polaritons, was a one-dimensional photonic wire. The geometry of this theoretical system is defined by the input number of molecules, $n_{mol,}$ and a uniform intermolecular distance, a. These terms are used to

define the length of the long axis of the cavity as well as the linear molecular density. The molecules were assumed to be arranged in an ordered fashion with a single intermolecular distance as the effect of translational disorder is minimal in comparison to energetic disorder. [30]

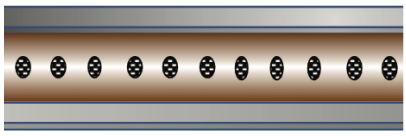

Figure 5. General schematic for molecular placement within the photonic wire. [30]

This geometry is supplemented by a wavevector space, the cavity photon modes are characterized by their wavevector or momentum along the long axis. These exists an equal number of positive and negative wave-vectors corresponding to positive and negative momenta. Throughout all of the calculations performed, the number of molecules was always set equal to the number of wavevectors within the system. This balancing of states increased computational costs but also assured that a sufficient number of cavity modes was always present regardless of the size of the system, even if the dominant resonant couplings only occurred with the lower energy wavevectors, fostering a truly multimode system.

The use of a single dimension within this photonic wire model effectively allows for a computationally, inexpensive system that can accurately represent the complexity of realistic polaritonic systems. [30] This will dramatically aid in the refinement of computational modeling of these quantum optical systems. The photonic wire model provides specific insight into confined cavity modes which can increase the understanding of the role and associated dynamics of cavity electromagnetic field distributions, to better understand how they facilitate polariton formation. [36]

2.1.2 Molecular System

This single dimension photonic wire model is filled with an ordered molecular ensemble that exhibits various properties and phenomena. As was discussed in Chapter 1, there are many competing processes which dictate the internal dynamics of energy exchange within optical microcavities. Most notably, these are the processes of energy exchange between light and matter, the loss of energy through a molecular loss of coherence, and the loss of energy through photonic escape or leakage from the cavity itself. The first of these three is the light-matter coupling, and the latter two give rise to damping. These are two competing processes within optical microcavities that determine the regime of the interactions between the molecular material and its host cavity.

Most theoretical and computational investigations into the intricacies of not only energy transfer dynamics but also that of other cavity phenomena include mathematical additions to the system that modulate the damping processes. Despite the relevance of these terms in properly expressing the system, they are generally considered to be of minimal importance when the system is under the strong coupling regime. [21] This regime is identified by the coupling process being much greater in magnitude than that of damping. All calculations were conducted under the strong coupling regime and consequently these terms were not included as to simplify the computational model. In addition to the added simplicity of the system, the exclusion of energy dissipation allows for a more thorough analysis of quantum intermolecular energy transfer dynamics in the best-case scenario where the system shows no energy, nor coherence losses.

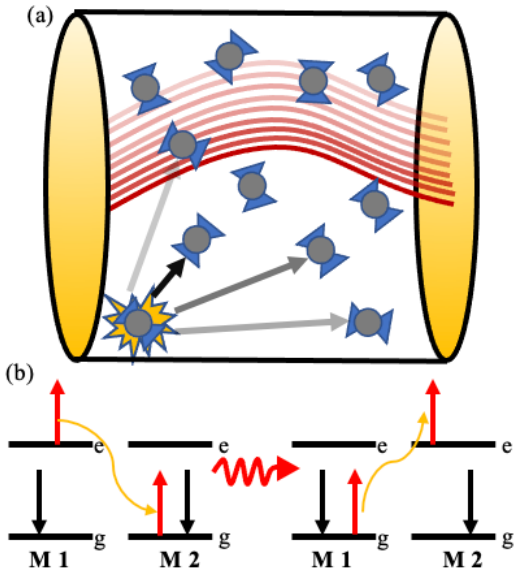

Figure 6. (a) Schematic for energy transfer in an optical microcavity. (b) Excited state energy transfer between two molecules of the same chemical composition.

Various types of disorder can exist within the study of polaritonic systems, for example: energetic disorder and translational disorder. Typically, energetic disorder dominates unless it is very small [Ribeiro], therefore we ignore translational disorder. This resulted in the uniform placement of the molecules with fixed intermolecular distances, and the simplification of the calculation of the energy diffusion in the molecular subsystem. The presence of energetic disorder among the molecular ensemble is one of the major novelties of this work. This disorder arises from the fact that molecules generally lie in a disordered phase in an optical cavity and the local environment of each molecule can vary substantially.

The molecular ensemble disorder originates from a specific input term, σ. This term is associated with the variance in a Gaussian distribution. This distribution is sampled to assign the values of the molecular excitation energies to each of the molecules within the system. The Gaussian is centered at the input mean molecular excitation energy, and the inclusion of a non-zero variance for this function allows for a certain spread of molecular excitation energies. This spread is intended to mimic the alterations in the local surroundings of each molecule and is

reflected in the resulting fluctuation of a molecular excitation energy relative to the average. The probability distribution for which the model samples energies from is given by the expression in Equation 3.

$$P(x) = e^{-\frac{(x-\mu)^2}{2\sigma^2}} \tag{3}$$

When a given calculation exhibits the effects of energetic disorder, the system, as generated by the Hamiltonian, undergoes *molecular ensemble averaging*. This is a necessary function as the generated disorder is sampled from a distribution function and consequently has many random internal processes. As a result, the model uses a singular disordered Hamiltonian, but realizes this system through time-evolution various times. This process uses different initial states located across the cavity that are similarly sampled. These realizations allow for the transport phenomena across the system to be evaluated. This avoids the skew that can be yielded from a small number of samples with localized initial states. These multiple realizations are then averaged with standard deviations to present a holistic view of energy transport dynamics within the cavity.

2.2 Hamiltonian Definition

All calculations performed in this project were conducted using Python 3 and Jupyter notebooks. [32,33] These computations and resulting figures also employed the Python 3 computational packages NumPy and Matplotlib. [34,35] These computational tools were used to generate all relevant code and theoretical models. The cavity Hamiltonian employed in this project consists of a one-dimensional photonic wire that i describes the standing waves of the cavity. This photonic wire, shown in Figure 5, has uniformly distributed target molecules

throughout its single long axis. Each molecule interacts with the cavity through their dipole which is assumed to be equal for simplicity. The formulas for the bare molecular and photonic subsystems of the cavity are expressed in Equations 4, 5 and 6 below, where q is defined as a photonic wavevector (momentum) along the long-axis, i is defined as a molecule, E_o is the mean molecular excitation energy, and σ_i the random Gaussian fluctuation in the excited-state energy for a molecule in the ensemble. Additionally, the bounds of n_{phot} and n_{mol} employed in Equations 4, 5, 6, and 7 are indicative of the maximum number of wavevectors and molecules respectively, within the system. The values of a_q and $a^\dagger_q$ denote the photon annihilation operator and the photon creation operator respectively, for wavevector q. These terms are similarly reflected by the molecular subsystem in Equation 6, where b_i and $b^\dagger_i$ indicate the excited state annihilation operator and the excited state creation operator respectively, for molecule i.

$$H_{Photonic} = \sum_{q=0}^{n_{phot}} \hbar\omega_q a_q^\dagger a_q \tag{4}$$

$$\omega_q = \frac{c}{n_{phot}}\sqrt{q_0^2 - q^2} \tag{5}$$

$$H_{Molecular} = \sum_{i=1}^{n_{mol}} (E_0 + \sigma_i) b_i^\dagger b_i \tag{6}$$

$$H_{Coupling} = -i\sum_{m}^{n_{mol}}\sum_{q}^{n_{phot}} \frac{\Omega_R}{2}\sqrt{\frac{\omega_o}{n_{mol}\omega_q}}(e^{iqx_m} b_m^\dagger a_q - e^{-iqx_m} a_q^\dagger b_m) \tag{7}$$

$$\widehat{H} = \widehat{H}_{Photonic} + \widehat{H}_{Molecular} + \widehat{H}_{Coupling} \tag{8}$$

Equation 8, above, indicates how the bare subsystems are combined with a light matter coupling term, shown above in Equation 7. Within the coupling term, Equation 7, the Ω_R is the

light-matter coupling strength of the system, and the terms that use the aforementioned operators facilitate the interactions between the light and matter of the system. This Hamiltonian matrix is then diagonalized using NumPy linear algebra functions to yield both an eigenstate column vector that contains the energies of all eigenstates of the system, as well as an eigenvalue matrix that contains all molecular and photonic coefficients of the system at every eigenstate. This output column vector and coefficient matrix are represented below in Equations 9 and 10.

$$\begin{bmatrix} E_0 \\ E_1 \\ E_2 \\ \vdots \\ E_n \end{bmatrix} \tag{9}$$

$$\begin{bmatrix} c_{i_1,E_0} & c_{i_1,E_{\dots}} & c_{i_1,E_n} \\ c_{i\ ,E_0} & \ddots & \vdots \\ \vdots & & \\ c_{i_{nmol},E_0} & \ddots & \vdots \\ c_{q_1,E_0} & \ddots & \vdots \\ c_{q\ ,E_0} & \ddots & \vdots \\ \vdots & & \\ c_{q_{nphot},E_0} & c_{q_1,E_{\dots}} & c_{q_1,E_n} \end{bmatrix} \tag{10}$$

2.3 Time Evolution

Another novel aspect of these calculations is found within the time dependent evolution. This functionality allows for the visualization of the dynamics of the system, sampled from various time scales, using different resolutions. A function was constructed to perform the time-evolution which requires as input the total evolution time and the number of time steps where a snapshot of the state of the system is recorded. The system is generally evolved by the

mathematical expression shown in Equation 11. This equation demonstrates that the Hamiltonian operator can work on a given time evolving wavefunction to produce its associated eigenstate value.

$$\widehat{H}\psi(t) = i\hbar\partial_t\psi(t) = E\psi(t) \tag{11}$$

This portion of the code uses the computed eigenvalues of the system, as well as the molecular and photonic coefficients corresponding to each eigenstate of the Hamiltonian to give time evolved coefficients that can be used to determine the probability of finding energy stored in a given molecule or cavity mode at a given point in time. This process was separated into two parts that track the molecular and cavity subsystems. The time-dependent coefficients are respectively given by Equations 12 and 13, below.

$$c_m(t) = \sum_{\alpha=0}^{N_s} \sum_{m=0}^{Nm-1} e^{\frac{-iE_\alpha t}{\hbar}} c_{m\alpha} c_{\alpha\phi} \tag{12}$$

$$c_{q_n}(t) = \sum_{\alpha=0}^{N_s} \sum_{n=0}^{Nc-1} e^{\frac{-iE_\alpha t}{\hbar}} c_{q_n\alpha} c_{\alpha\phi} \tag{13}$$

In Equation 12, the N_s term indicates the total number of states within the system, m is the index of a specific molecule, N_m is the total number of molecules in the system, α indicates the index of an eigenvalue, E_α is used to indicate a specific eigenvalue, and $c_{\alpha\varphi}$ denotes coefficient of the overlap a given eigenstate with the initial state that of the evolution. This overlap is generated by taking the dot product of the summation of all molecular and cavity

states for an eigenstate with the normalized column vector that represents the initial state. These values are also represented in Equation 13 for the cavity subsystem, with the addition of n indicating the index of a specific cavity mode and N_c being the total number of cavity modes present within the system. The implementation of these two equations allows for the generation of time evolved coefficients for each molecule and cavity mode. These coefficients are then used with Equation 14 and 15, below, to generate the time evolved probabilities for every molecule and cavity mode within both subsystems.

$$P_{m\phi}(t) = |c_m(t)|^2 \tag{14}$$

$$P_{q_n\phi}(t) = |c_{q_n}(t)|^2 \tag{15}$$

2.4 Initial State

The initial state is an incredibly important aspect of the computational model as it indicates the distribution and partition of the energy between the cavity and the molecules at time zero. There are many possibilities for initial energy locations or initial states that can be used with polaritonic cavity systems. This specific model employs the use of a Gaussian Molecular Excited State.

The use of a Gaussian Molecular Excited State indicates that the energy at time zero, is initially located within a Gaussian distribution of neighboring molecular excited states. This excited state is defined by a normalized column vector. This distribution is defined by the expression shown in Equation 16 below.

$$f(x) = \frac{1}{\sqrt{2\pi\sigma^2}} e^{-\frac{(x-\mu)^2}{2\sigma^2}} \tag{16}$$

The center of this distribution is described by the value μ, the variance of the function is defined by σ. The μ value of the system changes in a process known as statistical ensemble averaging, which will be discussed in further detail in later chapters. Across all simulations the σ value is universally set to two. This value causes the initial excited-state to be delocalized across nine molecules. We choose a weakly delocalized initial-state as it has smoother evolution relative to a single-molecule; furthermore, laser pulses are generally Gaussian shaped, and the excited-states generated by such are Gaussian wave packets. All of the excited-state coefficients are positive and normalized indicating that they are all in phase with one another.

2.5 Energy Transport Observables

Throughout this investigation, there were many different parameters of this computational model which were evaluated in determination of their impact on energy transport. This section details the various processes and their associated computations that were employed to study this model.

The tracking of the energy diffusion within the optical microcavity is a core feature of the mathematical model and serves to effectively measure the rate of energy diffusion of the polaritonic system under a variety of conditions. This facilitates the novel study of cavity effects on intermolecular energy diffusion. The functionality of our code tracks the energy flow in molecules within the cavity, as facilitated by the quantum light matter coupling phenomena. The created function assigns positions to all of the molecules within the system using their molecular index within this subsystem as well as the intermolecular distance to establish the cavity geometry. This expression is demonstrated in Equation 17.

$$x_i = \sum_{i=1}^{N_{mol}} ia \tag{17}$$

The energy transport across the molecular system is tracked by the mean squared displacement from the average position of the initial state as described in Equation 18 below. Delta x is the displacement, x_0 indicates the average position of the initial state of the wave packet, and $P_m(t)$ is the time evolved probability for molecule m.

$$< x^2(t) >= \sum_{m=1}^{N_m} P_m(t)(x_m - x_0)^2 \tag{18}$$

2.5.1 Short-time Propagation

Based on the existing lack of understanding in the short time dynamics of energy transfer and the role played by dark states in this process, these first simulations sought to determine the characteristics of the energy flow in the molecular subsystem at early times. This computation uses varying values of light-matter coupling, Ω_R, and determines their impact on the spatially-resolved transport of energy within the system. This procedure evaluates the increased light-matter coupling by the proportional relationship of displacement to time and quantifies this through the calculation of the slope. The impact of increasing Ω_R is evaluated using the values 0.1 eV, 0.3 eV, and 0.5 eV. No energetic disorder was included in these computations as we examine its effect later. These calculations were performed for intermolecular distances of 10, 20, and 30 nm. T Energy transport was tracked in the molecular subsystem for the first 500 femtoseconds of its evolution. Additionally, the early time scale of these calculations was evaluated to determine its diffusivity. This was accomplished through the calculation of the slope of the points of the early times, using linear fitting; these values are indicated within the caption of Figure 9. These calculations were also supplemented by functions that mapped the molecular and cavity photon probabilities of finding the energetic excitations within the molecular or cavity

subsystem. These supplemental calculations provide insight on the nature of the diffusivity and comment on the role played by the molecules and dark states within this system.

2.5.2 Diffusion Constant

The main observable evaluated within this investigation is the energy diffusion constants. This process was facilitated by the utilization of the formulas indicated in Equations 1 and 2, within Chapter 1. In order to calculate the diffusion constant *D* and the effective velocity *v*, the squared displacement discussed in *2.5* was divided by double the values of the time. This process yielded the diffusion constants as the slope of the resultant functions.

$$D = \frac{\Delta x^2}{2t} \tag{19}$$

Despite this linear fitting of the produced data, shown in Equation 19, there appeared to be diffusive dynamics within the early time evolutions of the system which did not match that of the later times of the system. This phenomenon was exacerbated by systems with no energetic disorder; this is demonstrated by the differing diffusive regimes shown in Figure 7. In order to properly accommodate for these differences, the diffusion constants for the system were calculated within the later time diffusive regimes which demonstrated linear increases. This was by applying a percentage-based threshold, which only used the final 10% of values to calculate the diffusion constant. The final 10% of values were calculated on a total time scale of 20ps, and as evidenced by the location of the transport regimes in Figure 7, this was always located in the diffusive regime. This procedure assured that the calculation of the diffusion constants only used the later-time regime, diffusive regime.

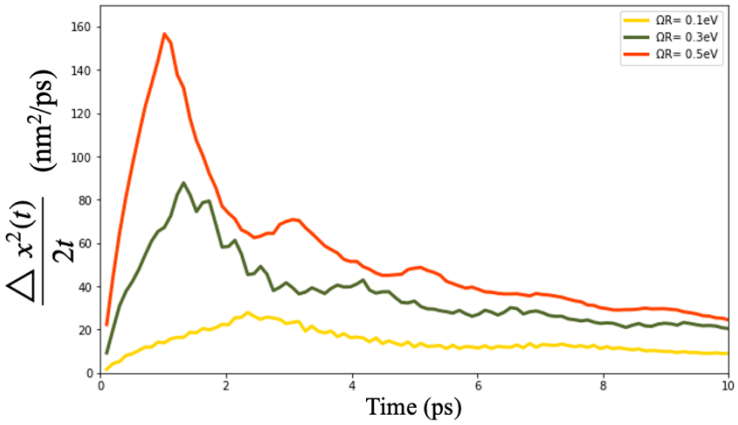

Figure 7. Indication of two general diffusive regimes. This is a calculation of the time-evolved displacement squared divided by two times time versus time. This calculation has no energetic disorder, no system detuning, uses an Ω_R values of 0.3eV, and an intermolecular distance of 100nm.

In this Section, the intermolecular energy transport dynamics at timescales where the motion follows the diffusion law shown in Equation 2. Diffusion constants are reported as a function of the light-matter interaction strength. Imperfections of real systems are incorporated in simulations by making the energetic disorder different from zero. In particular, diffusion constants are computed for several values of the light-matter coupling strength but the ratio of energy fluctuation variance to Rabi splitting (σ/ΩR) was maintained. For this calculation, as well as all others with introduced energetic disorder, *statistical ensemble averaging* was performed. In these simulations, the eigenstates of a single Hamiltonian with energetic disorder is first obtained, time-evolution of twenty-five initial molecular wave packets of the Hamiltonian realization are propagated, and the average diffusion constant obtained for each initial-state is computed. This process is employed in order to return a general understanding of the diffusive dynamics of the system. This limits the localization effects by energetic wells within the system

that can misrepresent diffusive dynamics. In order to demonstrate this averaging process, standard deviations have been included within this calculation on all of the plotted points.
In previous experiments of similar design, fairly misunderstood observables were measured in correlation to system size, to determine their internal system dynamics and begin to understand their internal functionalities. [17] As a result, there exists significant interest in the definition of the impact of system size on the novel observable of this investigation, real space energetic diffusion. In order to determine this, calculations comparing the impact of diffusion constants as a function of increasing the total number of states, collective number of molecules and photonic modes, of the system was used as a model. This process employs systems which have an equal number of both cavity modes and molecules, to preserve a symmetric multimode model. These calculations employed the process of *statistical ensemble averaging.* In order to define the impact that the energetic system disorder has on this calculation, the system disorder was run over two separate proportions.

Demonstrated by the previous experiments, energetic disorder among the molecular ensemble plays a driving role in the determination of the diffusivity of energy within an organic, polaritonic, optical microcavity system. In order to further describe these phenomena, increasing the proportion of disorder to light-matter coupling strength, Ω_R/σ, was plotted against its associated diffusion constants. This process employed *statistical ensemble averaging*, and was used for two separate functions that describe values of σ/Ω_R that are greater than 1, and values of Ω_R/σ that are less than 1. The evaluations of these two regimes effectively indicates both the threshold disorder values where the light-matter coupling becomes overcome by the strength of the energetic disorder, and the regime where the disorder strength is less than that of the light-matter coupling.

3. Ideal System

3.1 Introduction

Within any computational system there is large dependence on the theoretical and mathematical design of the system. Through various investigations into the processes of organic microcavity polaritonic systems there have been different evaluations of energetic movement and transfer. As a result of largely varying methodologies there have been some conflicting understandings in the function of various parameters of these polaritonic cavities. To standardize these internal parameters, this original system model evaluates energy transport within a set of idealized parameters, that are defined by the absence of energetic disorder among the molecular ensembles.

While the formation of light-matter hybrid states, polaritons, is an essential aspect of chemistry in optical microcavities, there exists also a large number of molecular states, known as *dark states*, which are only weakly coupled to the confined cavity field. There is a growing consensus in the large diffusive dependence on the dynamics of the molecular dark states, or excitons. [21,17] These states are extremely difficult to study experimentally because, as their name implies, they are dark and cannot be easily detected with optical spectroscopy techniques. There has been evidence of energetic localization within these dark states. [21] The coherent energy transport within the molecular dark states remains a gap in the understanding of these complex systems. At very short time scales, there is increased desire to study dark states within the picosecond and sub-picosecond regimes. [21]

There remains a general lack in agreement and understanding of diffusive dynamics of energy within microcavity polaritonic systems. Consequently, there is very little information

regarding the intricacies of short time dynamics. Due to the incredible difficulty of extremely small, time resolution required for experimental work at short times, theoretical models must aid in the guidance and detailing of these systems. Through the proper modeling of an idealized system with sufficiently complex properties these phenomena can effectively be investigated. Short time scales, however, require that the model in use realizes through many iterations; this greatly increases the computational costs, but it also facilitates the understanding of dark state dynamics.

In order to determine the impact of varying system parameters on the energy diffusion at ultrafast (femtosecond) time scales, the light-matter coupling strength of the systems were varied. The variance of these light-matter coupling strength, or Rabi Splitting (Ω_R) values, was employed to understand not only ballistic transport but also the impact of coupling strength on energy transport at longer times (picoseconds).

3.2 Ballistic Motion

In the evaluation of early-time dynamics, the methods outlined within *2.5.1* were employed to generate and define short-time ballistic trajectories. These trajectories can effectively be compared by the values of their slopes described within the caption of Figure 8.

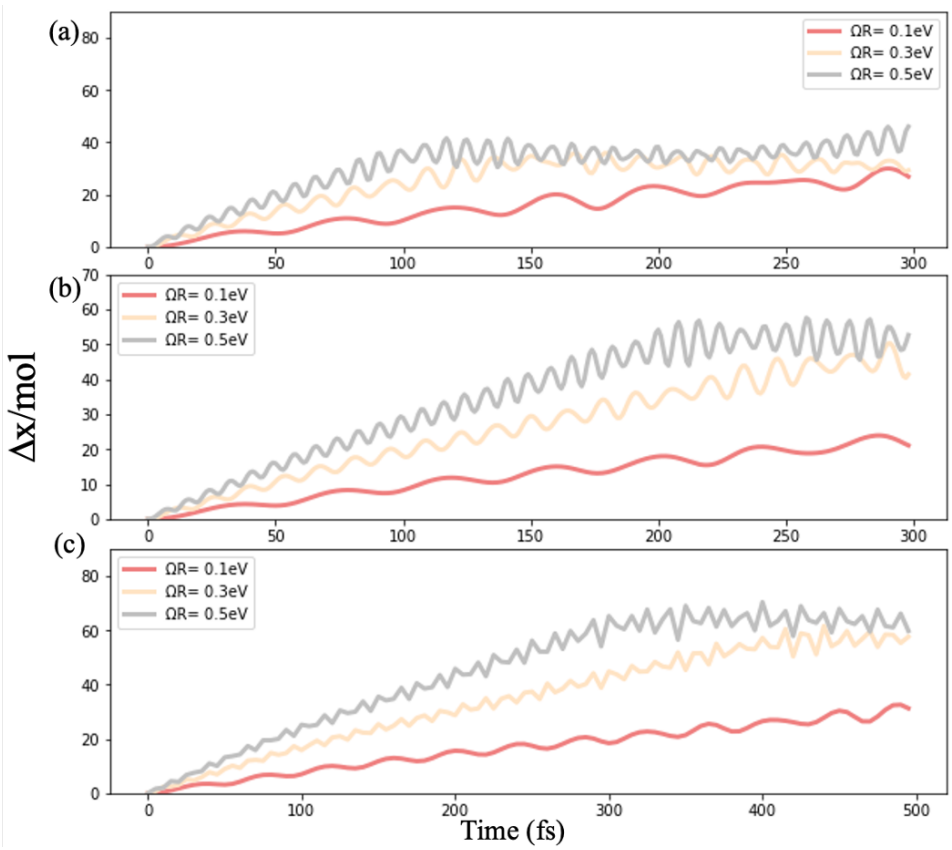

Figure 8. Ballistic energy transport for varying values of Ω_R within the short-time scale calculations. (a) Mean eave-packet displacement trajectories for a system with 10nm intermolecular distance. The short-time slopes for 0.1, 0.3, and 0.5 eV values of Ω_R, are 0.6534, 0.9752, 1.459 respectively, in units of molecules per femtosecond (10nm/fs). The slopes were calculated using the first 100fs in a linear fit. (b) Trajectories for a system with 20nm intermolecular distance. The short-time slopes for 0.1, 0.3, and 0.5 eV values of Ω_R, are 0.6410, 1.564, and 2.100 respectively, in units of molecules per femtosecond (20nm/fs). The slopes were calculated using the first 200fs in a linear fit. (c) Trajectories for a system with 30nm intermolecular distance. The short-time slopes for 0.1, 0.3, and 0.5 eV values of Ω_R, are 0.9983, 2.298, 4.120 respectively, in units of molecules per femtosecond (30nm/fs). The slopes were calculated using the first 300fs in a linear fit. All of these calculations were carried out with 501 molecules and zero detuning.

Demonstrated by the data presented within Figure 8, increasing both the value of the light matter coupling, as well as the intermolecular distance seems to have a significant impact on the diffusivity of the energy within the molecular subsystem of the cavity. Based on the increasing values of the slope for the different values of Ω_R within each of the three plots, there does appear to be a proportional correlation to increasing the strength of the light-

matter coupling, observed by increasing the rabi splitting value, and its impact on the diffusivity of the energy. Despite this proportional relationship, it does not appear to be a linearly correlated system. This is likely a result of the complexity of the system and the interdependence of diffusivity on many varying aspects of the cavity dynamics. This result develops from the inherent increase of light-matter coupling within the system. The strength of the light-matter interaction within this system is indicative of the amount of delocalization between molecular and photonic characteristics. These enhanced phenomena aid in the transfer dynamics of the energy within the cavity, as photonic components have a higher capacity for energetic transfer than that of molecules. These simulations serve to demonstrate the important role played by the light-matter coupling strength of a polaritonic optical microcavity system in augmenting its energy transport speed.

3.3 Subsystem Energy Localization

The investigation of idealized ballistic energy transport was supplemented by the information provided in Figure 9. These calculations sought to demonstrate the probability of finding the energy within the molecular and cavity subsystems as a function of time. This calculation indicates 1) in which subsystem the energies are mainly situated within the cavity at the given time steps, as well as 2) the relative importance of the molecules and cavity modes in the energy transfer dynamics of the system.

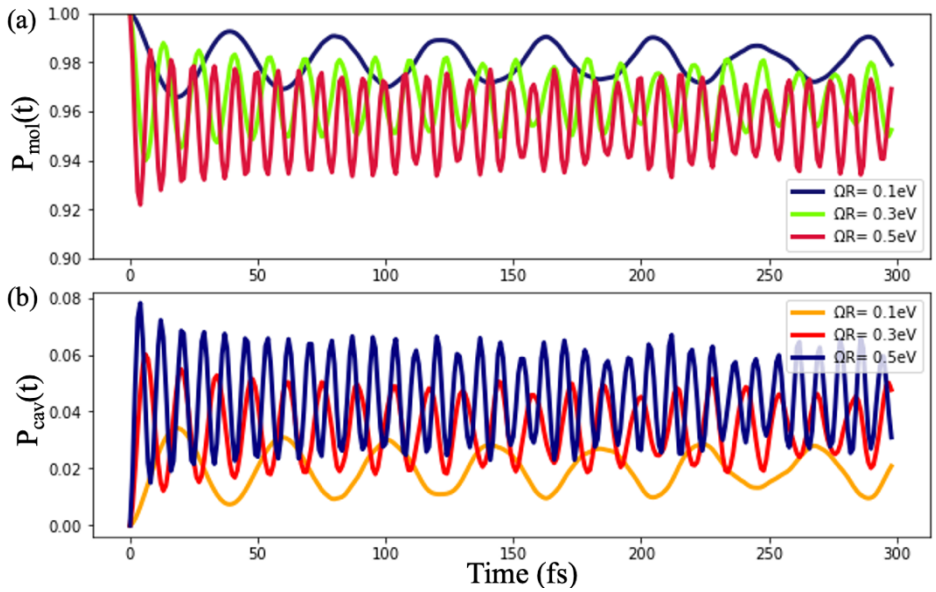

Figure 9. Time evolved subsystem probabilities for short-time ballistic energy transport. Demonstrates the probability of finding the energetic excitations within (a) the molecular subsystem and (b) the cavity subsystem. These calculations have Ω_R = 0.1,0.3,0.5 eV, no energetic disorder, 501 molecules, bare molecular excitation energy of 2.0eV, and an intermolecular distance of 20nm.

As evidenced by the data provided in Figure 9, there is significant energetic localization within the cavity during these early times. This trend is observed, most notably, by the large molecular subsystem probabilities and the small values for that of the cavity. This indicates that short-time observations emphasize a very strong molecular contribution to cavity dynamics. Additionally, these calculations were performed within a system that is experiencing no energetic disorder. Since energetic disorder is largely associated with energetic localization effects, through the molecular subsystem, this result may demonstrate an increased importance for the understanding of molecular contributions to all cavity phenomena. [17] This molecular localization within dark states further solidifies the integral

elucidation of their energy transport properties. This reinforces the underlying dependence of dark states in the internal function of microcavity systems and their associated energy transport and chemistry as explained by Raj et al. [21]

Despite the extreme energetic localization within the molecular subsystem, as indicated within Figure 9, there are still significant oscillations within both the molecular and cavity time-evolved probabilities. These fast oscillations are indicative of the interplay between the subsystems, showing that energy transport is modulated by photonic contributions known as virtual excitations. This reinforces the light-matter coupled nature of the system and its facilitation of energy exchange.

4. Microscopic Models with Disorder

4.1 Introduction

As evaluated in Chapter 3, there is significant dependence of a given computational model on the mathematical and theoretical framework that is used to structure its calculations. In addition to computational dependence, there is also significant reliance on the parameters of the polaritonic system itself. Within organic optical microcavities, the presence of energetic disorder is one of the major parameters that will aid in the enhancement of computational models and their resultant predictions. The existence of the polaritons within a disordered phase, inherently leads to the experimental exhibition of energetic disorder within the target molecules of the system. These energetic alterations are generally generated from the collisions and intermolecular interactions between the target molecules and both the solvent molecules and the structural molecules that make up the walls of the cavity. These alterations shift the mean molecular excitation energies away from that of their bare values. These shifts have been

associated with the production of weak photonic intensity and minor shifts from the Tavis-Cumming (TC) model system. [37] These shifts can result in the trapping of energy which will largely limit its diffusive capacity. This type of energetic disorder among the molecular ensemble has yet to be fully evaluated and included into many previous computational investigations. [17]

An important input that dictates a lot of the internal dynamics of the system is the number of states. These states are defined by the collective number of both molecules and cavity photon modes. The number of states is a largely important value as it largely impacts the interactions within a cavity. There is an internal uncertainty principle that correlates the number states to the dipole moment of each molecule. Therefore, as the number of states increases, each individual molecule contributes progressively less to the general dynamics of the system. As a result of this, the diffusive properties of the energy within systems of increasing size must be evaluated.

In similar experiments that measured different observables, the presence of molecular energetic disorder within calculations resulted in energetic localization. This was explained to be a result of Anderson localization, that the presence of any disorder in a one-dimensional system can result in energetic localization. [17] As a result of this, there is significant interest in exploring how the introduction of disorder to a system of increasing size impacts the diffusive capabilities of the system. Additionally, these previous experiments were conducted on an infinite time scale. [17] As a result of this computational difference, the variation in time scales between these calculations may aid in the elucidation of how shorter time regimes can differ in their impact on energetic localization, and dark state dynamics. These calculations seek to increase the number of states within the system and determine the impact on the energetic diffusivity.

As a result of the incredible importance of energetic disorder in yielding more representative theory and computations, this parameter was evaluated in reference to its impact on the energy diffusion of the system. Through the introduction of energetic disorder, the ballistic energy transport observed within the idealized model was no longer observed and the general system appeared to remain in the diffusive transport regime. As a result of this, only the diffusive behavior of disordered systems was evaluated. An additional important question regarding the presence of energetic disorder, is does increasing the amount of disorder, dramatically increase the energetic localization of the system or is a small amount of disorder sufficient to cause an effect.

4.2 Energy Transport Dependence on Light-Matter Coupling Strength

Following these fundamental observations, this computation sought to determine the role of increasing the light-matter coupling strength of the system with the introduction of constant disorder. This experiment mapped the diffusion constants of the system as a function of increasing rabi splitting, Ω_R, in order to effectively determine how the diffusivity of the system is altered through the presence of energetic disorder.

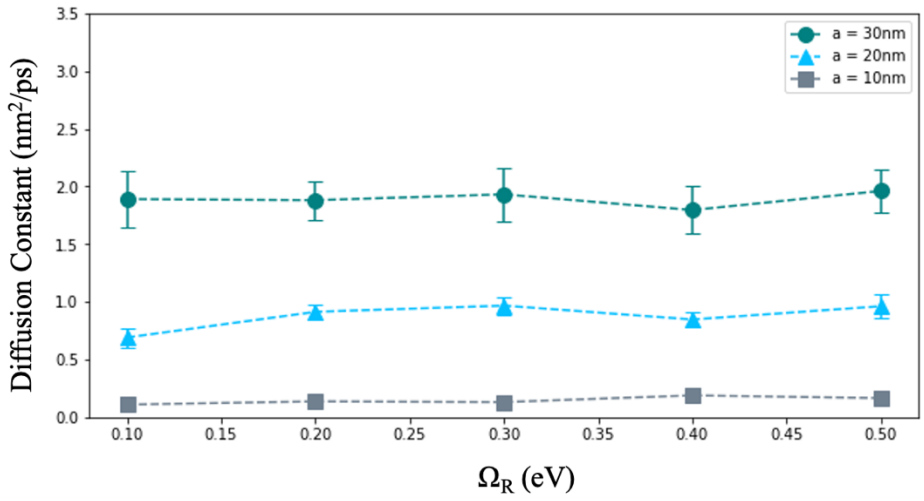

Figure 10. Diffusion constant as a function of light-matter coupling strength. Both Ω_R and the intermolecular systems were varied, while the number of molecules was kept fixed at 501, the bare molecule excitation energy at 2.0 eV, and $\sigma/\Omega_R = 0.01$. Each of the presented results correspond to averages over 25 molecular excited-state Gaussian wavepackets centered at a random molecule (standard deviations are represented by the bars at each point).

As demonstrated by the data presented in Figure 10, the introduction of disorder does alter some of the system dynamics. The trend returned by Figure 10, may initially appear to conflict with the trend demonstrated by the early time slopes derived within Figure 8. This conclusion could be drawn from the lack of increasing diffusion constants as the light-matter coupling strength of the system increases. Although these seemingly conflicting results appear to indicate a lack of phenomenological consistency, in fact, the trend demonstrated by Figure 10, seeks to show an entirely separate dependence. Although the value of Ω_R is becoming larger, the maintenance of the diffusion constants within this calculation indicates that instead of the dependence being limited to the value of Ω_R, it is now strictly dependent

on the proportion of σ/Ω_R, in systems with energetic disorder (where σ refers to the amount of energetic disorder of the system in units of eV). This demonstrates that the presence of energetic disorder within the investigation of system dynamics is an essential consideration.

4.3 Energy Transport Dependence on Number of Molecules

In order to determine the impact of the number of states on the energetic diffusion of the system, the system size was varied; these results are demonstrated in the plots shown in Figure 11.

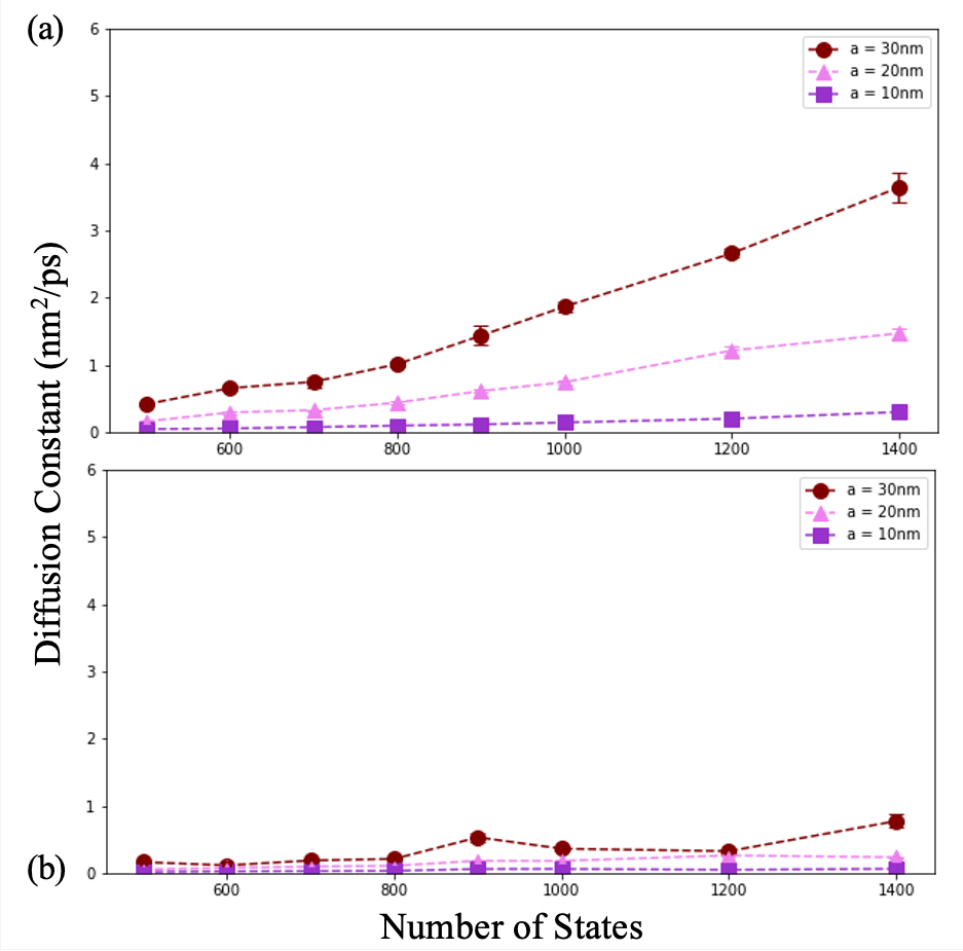

Figure 11. Diffusion constants as a function of the total number of states for intermolecular distances of a=30nm, a=20nm, and a=10nm. The total light-matter interaction was fixed at Ω_R =

0.3eV. (a) Simulation results obtained with $\sigma/\Omega R = 0.01$. (b) Simulation results obtained with $\sigma/\Omega R = 0.2$.

Demonstrated by the data in Figure 11, there appears to be a correlation between energetic diffusion and the size of the system. As the system size increases, the ability for the energy to move also appears to increase. This is an interesting finding, as previous experiments have evaluated some observables to reach a thermodynamic limit in which their observables converge to a stationary value. These previous findings have determined that phenomena, such as escape probabilities, have minimum system size requirements and after this threshold, converge. [17] Unlike these observables, real space energetic diffusion appears to have a significant dependence on the size of the system.

Despite this increased energy transport with increasing system size, there remains a specific balance in the weight of the system's parameters. As demonstrated by plot b in Figure 11, the increase in the proportion of σ/Ω_R from 0.01 to 0.2, still has a dramatic impact on the energy transfer dynamics of the system. This decrease in the values of the diffusion constants can be directly associated with the energetic localization, indicating that a higher magnitude of energetic fluctuations still prevails over the increased delocalization of larger system sizes. This indicates that although system size has proven to be an impactful parameter for energy transfer, the system is still dominated by the presence of energetic molecular ensemble disorder.

4.4 Diffusion Constants under Strong Disorder

Based on this damping of energy transport resultant from the investigation of system size, there is significant interest in determining the dynamics of increasing the presence of energetic

disorder. In order to evaluate the impact of large values of energetic disorder the diffusion constants were plotted against values of Ω_R/σ that are less than one. This was employed to determine different regimes of disorder, in which either the light-matter coupling, or the energetic disorder dominate the system. This threshold is facilitated by either energetic diffusion or energetic localization.

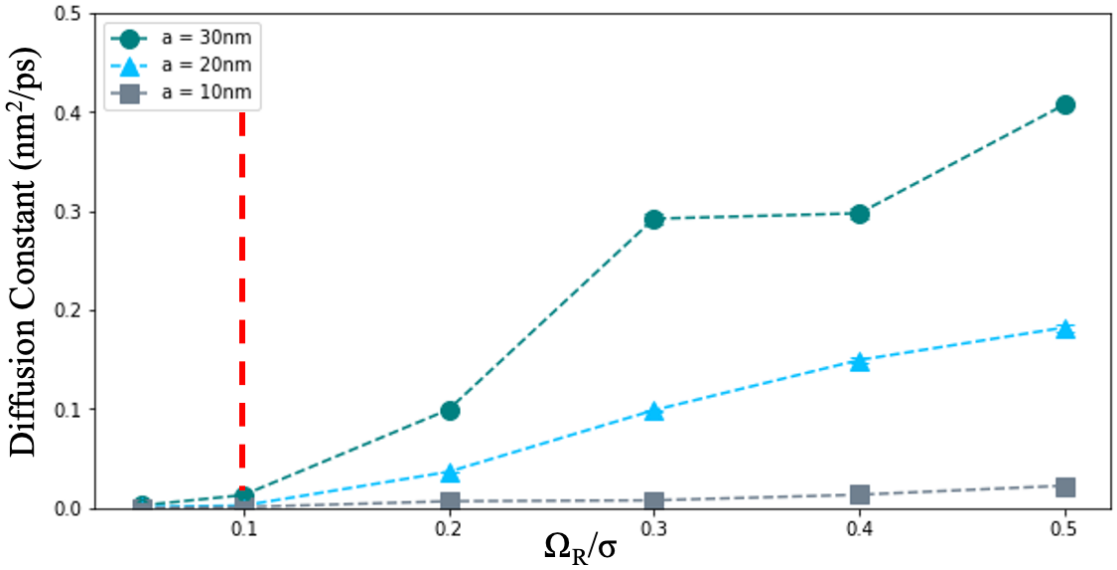

Figure 12. Diffusion constant under strong disorder where the light-matter interactions are weaker than the magnitude of molecular excited-state energy fluctuations, i.e., $\Omega_R/\sigma < 1$. The red vertical line indicates a rough threshold for the transition between the regimes of strong energy localization (where the diffusion constant is approximately zero) and a diffusive regime where the diffusion constant starts to become appreciably different from zero.

Demonstrated by the trends indicated in Figure 12, there are two distinct regimes of disordered calculations. There is a regime entirely controlled by the energetic localization resultant from values of energetic disorder that are significantly larger than that of the rabi splitting (Ω_R) of the system. This demonstrates in what proportion that this shift occurs. As

graphically demonstrated by the red line in Figure 12, this regime switch occurs at the value of $\Omega_R/\sigma = 0.1$. This threshold calculation also indicates that the energetic localization can entirely inhibit the energetic diffusive properties of the system, if of sufficient magnitude.

4.5 Diffusion Constants under Weak Disorder

A similar calculation was performed for the opposing regime. In this case the model employed values of Ω_R/σ that were greater than one. This process sought to determine how impactful the values of energetic disorder are on localizing the energy within the molecules of the system, while not entirely inhibiting energy transport.

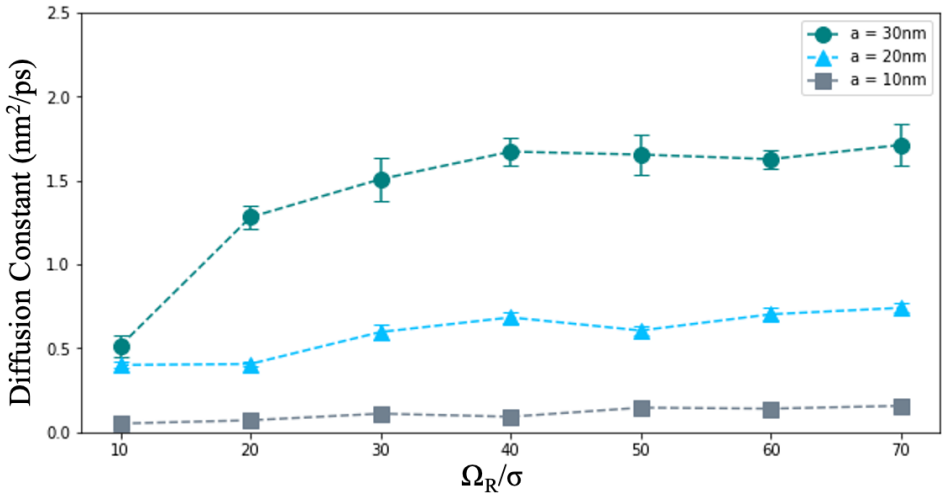

Figure 13. Diffusion constant under weak disorder where the light-matter interactions are stronger than the magnitude of molecular excited-state energy fluctuations, i.e., $\Omega_R/\sigma > 1$. These results show the generic trend that intermolecular energy diffusion becomes faster with weakening disorder.

Demonstrated by this secondary diffusive regime, shown in Figure 13, there is a gradual impact of increasing the energetic disorder on the diffusion within the system. For the system within smaller intermolecular distance, 10nm, this localization appears to resemble a linear trend. Despite this, moving to less densely packed systems, 20nm and 30nm, this localization is far more gradual. This difference is likely a result of the system densities and the density of states inequality, that is further detailed in 5. In addition to these levels of difference, all systems in Figure 13, demonstrate the general impact of introducing energetic disorder gradually and how it causes a proportional energetic localization within the molecular system, therefore inhibiting energetic diffusion.

The introduction of energetic disorder and the evaluation of system parameters generates many values for the diffusion constants, but these values largely lacked qualification. The investigation premise assumes that molecules outside of an optical microcavity generally exhibit no energetic diffusive properties and thus such diffusive phenomena are novel, and consequently greater than that of their classical counterparts. Despite this, some further classification of these results would aid in the understanding of the energy transfer speed of cavity systems and comment on their potential utility for applications. As a result of this, general cavity parameters were selected, and diffusion constants were calculated from this system. These calculated diffusion constants were compared to slightly different values from literature. It should be noted that these are novel diffusion constants, and that this comparison is between entirely different systems. The compared values are indicative of noncoherent energy transport, whereas this system evaluates the quantum or coherent diffusive case. [38] The values of the theoretical diffusion constants range approximately from 10^{-2} – 10^{-3} cm^2/s. These values coincide with literature values were diffusion constants evaluating noncoherent energy transport in perovskites.

[38,39] Based on this rough data classification in comparison to that of solid-state energy transfer, it is evident that the energy transport phenomena within the polaritonic optical microcavity is indicative of a very similar system. There are some minor differences within the values observed from the computational model. These differences may have arisen from the alterations in the intermolecular distances used.

5. Density Dependence

There is a strong uncertainty inequality connected to the density of states within the system that dominates the molecular contributions. By altering intermolecular distance, this changes the proximity of the molecules to one another and therefore skews the system's density. These density alterations have multiple potential impacts. Based on the uncertainty principle, shown in Equation 19, as the density of the system increases each individual molecule contributes significantly less to the light-matter coupling of the system; this is modulated through the change in magnitude of an individual molecules transition dipole moment. The following equation demonstrates the proportional uncertainty between the Rabi Splitting, Ω_R, and the single molecular dipole moment divided by the intermolecular distance.

$$\Omega_R \propto \sqrt{\frac{\mu^2}{a}} \tag{20}$$

This effect is easily seen through the inclusion of altering intermolecular distances in Figures 8, 10, 11, 12 and 13; as intermolecular distance increases, the diffusivity increases as well because each individual molecule is less impacted by the energetic disorder introduced. This reduction in impact is resultant from the increased dipole magnitude of the individual molecules in the molecular subsystem. A secondary understanding of the impact of state density is provided

through the functionality of the Hamiltonian. The interactions of the Hamiltonian are facilitated through the presence of an electric field. Since this field is spatially distributed, if there are many molecules in close proximity, they may begin to experience the same electric field and exhibit less difference. This can exacerbate localization with the addition of energetic disorder. Although this system operates under strong light-matter coupling, the use of a molecular excited initial state likely is the driving source of the similarity of these diffusion constants to that of noncoherent systems. Additionally, there has been some prospect that the presence of energetic disorder within these quantum systems can alter the forms of energy transport and result in seemingly noncoherent diffusion. Similar observations have also been made in highly ordered solid-state perovskite analysis and exciton movement. [39,40] Based on these results there is a significant basis to augment the understanding of the molecular subsystem within polaritonic optical microcavities.

Based on this rough data classification in comparison to that of solid-state energetic transfer, it is evident that the energetic transport phenomena within the polaritonic optical microcavity is indicative of a very similar system. There are some minor differences within the values observed from the computational model. These differences may have arisen from the alterations in the intermolecular distances used. As explained in *4.*1 there is a strong uncertainty inequality connected to the density of states within the system that dominates the molecular contributions. By altering intermolecular distance, this changes the proximity of the molecules to one another and therefore skews the system's density. These density alterations have multiple potential impacts. Based on the aforementioned uncertainty principle, as the density of the system increases each individual molecule contributes significantly less to the light-matter coupling of the system; this is modulated through the change in magnitude of an individual molecules

transition dipole moment. This effect is easily seen through the inclusion of altering intermolecular distances in Figures 9, 11, 12, 13 and 14; as intermolecular distance increases, the diffusivity increases as well because each individual molecule is less impacted by the energetic disorder introduced. This reduction in impact is resultant from the increased dipole magnitude of the individual molecules in the molecular subsystem. A secondary understanding of the impact of state density, is provided through the functionality of the Hamiltonian. The interactions of the Hamiltonian are facilitated through the presence of an electric field. Since this field is spatially distributed, if there are many molecules in close proximity, they may begin to experience the same electric field and exhibit less difference. This can exacerbate localization with the addition of energetic disorder. Although this system operates under strong light-matter coupling, the use of a molecular excited initial state likely is the driving source of the similarity of these diffusion constants to that of noncoherent systems. Additionally, there has been some prospect that the presence of energetic disorder within these quantum systems can alter the forms of energetic transport and result in seemingly noncoherent diffusion. Similar observations have also been made in highly ordered solid-state perovskite analysis and exciton movement. [26,27] Based on these results there is significant basis to augment the understanding of the molecular subsystem within polaritonic optical microcavities.

6. Summary and Conclusions

This investigation sought to define many of the novel dynamics of real space energy diffusion within short time scales of polaritonic optical microcavities in photonic wires. The various system parameters investigated sought to determine the roles played by the strength of light-matter coupling in both the ballistic and diffusive transport regimes, the total number of states in a given system, and the varying of energetic disorder strength.

The investigation into the idealized ballistic energy transport dynamics determined that there is extremely fast ballistic transport that occurs within short time scales. It is assumed that this initial transport regime is indicative of the high coupling of the molecular system to the cavity before it has had sufficient time to dephase. In addition to fast diffusion, the energy of the system is strongly localized within the molecular subsystem. This localization, however, is still accompanied by an energy transfer through the virtual excitations shown in Figure 9.

Through experimentation and computation, the strength of light matter coupling was altered in order to discern its impact on the energy transport capabilities of an organic, polaritonic, optical microcavity system. This procedure determined that there is significant dependence of diffusive dynamics on the strength of the light-matter coupling (Ω_R). Despite this conclusion, through the introduction of energetic disorder among the molecular ensemble demonstrated that this dependence on the light-matter coupling strength is also directly correlated to the amount of energetic disorder introduced to the system. This indicated that a pertinent system parameter is more accurately described by the proportion of energetic disorder to the strength of the light- matter coupling, σ/Ω_R.

Next this investigation intended to define the dependence of energetic diffusion on the size of the system as modulated by the number of total states. This experiment varied the number of total states of given systems and determined that increasing the size of the system has a direct correlation to increasing the energetic diffusion. This determined that energetic diffusion is consequently tied to system size. As the size of the system increased, the diffusion constants also grew in size. This result however was also compared to the same system with a significantly larger proportion of disorder introduced. This secondary qualification indicated that although these molecules are less impacted by the introduction of energetic disorder, there still remains a

strong localizing effect with high values of σ. This was shown by the dramatic increase in energy localization through the smaller diffusion constant values .

In response to the increasing impact of energetic disorder, the final direction of this investigation was to further qualify its role in energy localization. This final set of experiments employed varying proportions of Ω_R/σ and their associated diffusion constants to effectively determine energetically disordered regimes. This process saw that the threshold value of $\Omega_R/\sigma=0.01$, creates two separate energetic regimes, one dominated by energetic localization of the second that allows diffusive behavior. This threshold indicates that increasing values of energetic disorder can entirely alter the diffusive dynamics of the system and result in completely different diffusivity. This result was further evaluated with values of Ω_R/σ that are greater than 1. This calculation demonstrated varying proportional effects of decreasing disorder on the diffusivity of the system as correlated to the intermolecular distance of the system.

After these experiments, the results were taken and further qualified. The interest in understanding different diffusive regimes as a result of changing intermolecular distances was evaluated using the internal density of states uncertainty principle. The distance between molecules within the system contributes to their relative density within the cavity and therefore sees similar conclusions to those of the number of total states calculations. Consequently, as the intermolecular distance increases, each molecule is again not as impacted by the introduction of energetic disorder and exhibits higher diffusivity.

A qualification was performed on the diffusion constants produced from a general system. These were converted and compared to literature values of diffusion constants calculated within noncoherent energetic diffusion. Although this is not an exact comparison it began to provide some intuition to general diffusivity of the real space diffusion of these microcavity

systems. This comparison determined that the quantum phenomena observed in this photonic wire system experience relatively the same energetic diffusive properties as that of the classical system described in the literature. This conclusion indicates that the use of a molecular excited initial state has relatively similar properties to noncoherent systems. This result requires further investigation to identify exactly how this process is facilitated. Additionally, this conclusion places further interest on defining the case of a Lower Polariton initial wavepacket, and the energetic diffusivity of that system.

Although this project has begun to elucidate many previously unknown molecular and energetic phenomena within organic polaritonic, optical microcavities, there still remains many unexplored aspects of real space energetic diffusion at short-time scales. Additionally, there is significant interest in determining group velocities for systems in order to further understand their diffusive regimes. [21] The evaluation of various other initial states may aid in understanding other aspects of these systems whilst also providing opportunities for experimental comparisons. This will aid in the qualification of this computational model and seek to promote the understanding of these systems and their incredible potential for revolutionizing energy transfer. Finally, the addition of energetic disorder has seen the augmentation of this computational model, but there still must be further investigation on tuning other physically observed phenomena. The introduction of thermodynamic interactions with a heat reservoir to further elucidate the impacts of intermolecular interactions on the cavity-mediated energy transfer dynamics.

7. References

[1] Zhou, K.; Liu, Y.; Alotaibi, A.; Yuan, J.; Jiang, C.; Xin, J.; Liu, X.; Collins, B. A.; Zhang, F.; Ma, W. Molecular and energetic order dominate the photocurrent generation process in organic solar cells with small energetic offsets. ACS Energy Letters 2020, 5 (2), 589–596.

[2] Talawar, M. B.; Sivabalan, R.; Mukundan, T.; Muthurajan, H.; Sikder, A. K.; Gandhe, B. R.; Rao, A. S. Environmentally compatible next generation green energetic materials (gems). Journal of Hazardous Materials 2009, 161 (2-3), 589–607.

[3] Varnavski, O. P.; Ostrowski, J. C.; Sukhomlinova, L.; Twieg, R. J.; Bazan, G. C.; Goodson, T. Coherent effects in energy transport in model dendritic structures investigated by ultrafast fluorescence anisotropy spectroscopy. Journal of the American Chemical Society 2002, 124 (8), 1736–1743.

[4] Karki, K. J.; Widom, J. R.; Seibt, J.; Moody, I.; Lonergan, M. C.; Pullerits, T.; Marcus, A. H. Coherent two-dimensional photocurrent spectroscopy in a PBS quantum dot Photocell. Nature Communications 2014, 5 (1).

[5] Crabtree, G. W.; Lewis, N. S. Solar Energy Conversion. Physics Today 2007, 60 (3), 37–42.

[6] Morel, D. L.; Ghosh, A. K.; Feng, T.; Stogryn, E. L.; Purwin, P. E.; Shaw, R. F.; Fishman, C. High-Efficiency organic solar cells. Applied Physics Letters 1978, 32 (8), 495–497.

[7] Smestad, G. P.; Krebs, F. C.; Lampert, C. M.; Granqvist, C. G.; Chopra, K. L.; Mathew, X.; Takakura, H. Reporting solar cell efficiencies in solar energy materials and solar cells. Solar Energy Materials and Solar Cells 2008, 92 (4), 371–373.

[8] Blatt, J. M.; Böer, K. W.; Brandt, W. Bose-Einstein condensation of excitons. Physical Review 1962, 126 (5), 1691–1692.

[9] Xu, C.; Leonard, J. R.; Dorow, C. J.; Butov, L. V.; Fogler, M. M.; Nikonov, D. E.; Young, I. A. Exciton gas transport through Nanoconstrictions. Nano Letters 2019, 19 (8), 5373–5379.

[10] Ganesamoorthy, R.; Sathiyan, G.; Sakthivel, P. Review: Fullerene based acceptors for efficient bulk heterojunction organic solar cell applications. Solar Energy Materials and Solar Cells 2017, 161, 102–148.

[11] Orgiu, E., George, J., Hutchison, J. et al. Conductivity in organic semiconductors hybridized with the vacuum field. Nature Mater 14, 1123–1129 (2015). https://doi.org/10.1038/nmat4392

[12] Krainova, N.; Grede, A. J.; Tsokkou, D.; Banerji, N.; Giebink, N. C. Polaron photoconductivity in the weak and strong light-matter coupling regime. Physical Review Letters 2020, 124 (17).

[13] Polaritons https://www.nature.com/subjects/polaritons (accessed Mar 3, 2022).

[14] Basov, D. N., Asenjo-Garcia, Ana, Schuck, P. James, Zhu, Xiaoyang and Rubio, Angel. "Polariton panorama" Nanophotonics 10, no. 1 (2021): 549-577. https://doi.org/10.1515/nanoph-2020-0449

[15] Gross, E.; Permogorov, S.; Travnikov, V.; Selkin, A. Polariton emission from Crystals. Solid State Communications 1972, 10 (11), 1071–1074.

[16] Feist, J.; Galego, J.; Garcia-Vidal, F. J. Polaritonic chemistry with organic molecules. ACS Photonics 2017, 5 (1), 205–216.

[17] Ribeiro, R. F.; Martínez-Martínez, L. A.; Du, M.; Campos-Gonzalez-Angulo, J.; Yuen-Zhou, J. Polariton Chemistry: Controlling molecular dynamics with optical cavities. Chemical Science 2018, 9 (30), 6325–6339.
[18] Herrera, F.; Owrutsky, J. Molecular polaritons for controlling chemistry with Quantum Optics. The Journal of Chemical Physics 2020, 152 (10), 100902.
[19] Krasavin, A. V.; Zayats, A. V.; Zheludev, N. I. Active control of surface plasmon–polariton waves. *Journal of Optics A: Pure and Applied Optics* **2005**, *7* (2), S85–S89.
[20] Shalabney, A.; George, J.; Hutchison, J.; Pupillo, G.; Genet, C.; Ebbesen, T. W. Coherent coupling of molecular resonators with a microcavity mode. *Nature Communications* **2015**, *6* (1).
[21] Raj, Pandya et al. "Tuning the coherent propagation of organic exciton-polaritons through dark state delocalization." *arXiv preprint arXiv:2112.02141* (2021).

[22] Holmes, R. J.; Kéna-Cohen, S.; Menon, V. M.; Forrest, S. R. Strong coupling and hybridization of Frenkel and Wannier-Mott excitons in an organic-inorganic optical microcavity. *Physical Review B* **2006**, *74* (23).

[23] Finlayson, C. E.; Ginger, D. S.; Greenham, N. C. Enhanced förster energy transfer in organic/inorganic bilayer optical microcavities. *Chemical Physics Letters* **2001**, *338* (2-3), 83–87.
[24] Agranovich, V. M.; Gartstein, Y. N. Nature and dynamics of low-energy exciton polaritons in semiconductor microcavities. *Physical Review B* **2007**, *75* (7).
[25] Yu, M.-W.; Ishii, S.; Li, S.; Ku, J.-R.; Yang, J.-H.; Su, K.-L.; Taniguchi, T.; Nagao, T.; Chen, K.-P. Quantifying photoinduced carriers transport in exciton–Polariton coupling of Mos2 monolayers. npj 2D Materials and Applications 2021, 5 (1).
[26] Hutchison, J. A.; Schwartz, T.; Genet, C.; Devaux, E.; Ebbesen, T. W. Modifying chemical landscapes by coupling to vacuum fields. Angewandte Chemie International Edition 2012, 51 (7), 1592–1596.

[27] Thomas, A.; Lethuillier-Karl, L.; Nagarajan, K.; Vergauwe, R. M.; George, J.; Chervy, T.; Shalabney, A.; Devaux, E.; Genet, C.; Moran, J.; et al. Tilting a ground-state reactivity landscape by vibrational strong coupling. *Science* **2019**, *363* (6427), 615–619.

[28] Coles, D. M.; Somaschi, N.; Michetti, P.; Clark, C.; Lagoudakis, P. G.; Savvidis, P. G.; Lidzey, D. G. Polariton-mediated energy transfer between organic dyes in a strongly coupled optical microcavity. Nature Materials 2014, 13 (7), 712–719.
[29] Xiang, B.; Ribeiro, R. F.; Du, M.; Chen, L.; Yang, Z.; Wang, J.; Yuen-Zhou, J.; Xiong, W. Intermolecular vibrational energy transfer enabled by microcavity strong light–matter coupling. Science 2020, 368 (6491), 665–667.

[30] Ribeiro, Raphael F. "Strong light-matter interaction effects on molecular ensembles." *arXivpreprint arXiv:2107.07032* (2021)

[31] Del Pino, J.; Feist, J.; Garcia-Vidal, F. J. Quantum theory of collective strong coupling of molecular vibrations with a microcavity mode. *New Journal of Physics* **2015**, *17* (5), 053040.

[32] Van Rossum, G., & Drake, F. L. (2009). Python 3 Reference Manual. Scotts Valley, CA: CreateSpace.

[33] Kluyver, T., Ragan-Kelley, B., Fernando P'erez, Granger, B., Bussonnier, M., Frederic, J., … Willing, C. (2016). Jupyter Notebooks – a publishing format for reproducible computational workflows. In F. Loizides & B. Schmidt (Eds.), Positioning and Power in Academic Publishing: Players, Agents and Agendas (pp. 87–90).

[34] Harris, C. R., Millman, K. J., van der Walt, S. J., Gommers, R., Virtanen, P., Cournapeau, D., … Oliphant, T. E. (2020). Array programming with NumPy. *Nature*, *585*, 357–362. https://doi.org/10.1038/s41586-020-2649-2

[35] Hunter, J. D. (2007). Matplotlib: A 2D graphics environment. *Computing in Science & Engineering*, *9*(3), 90–95.

[36] Kuther, A.; Bayer, M.; Gutbrod, T.; Forchel, A.; Knipp, P. A.; Reinecke, T. L.; Werner, R. Confined optical modes in photonic wires. *Physical Review B* **1998**, *58* (23), 15744–15748.

[37] Houdré, R.; Stanley, R. P.; Ilegems, M. Vacuum-field rabi splitting in the presence of inhomogeneous broadening: Resolution of a homogeneous linewidth in an inhomogeneously broadened system. *Physical Review A* **1996**, *53* (4), 2711–2715.

[38] Kunsel, T.; Jansen, T. L.; Knoester, J. Scaling relations of exciton diffusion in linear aggregates with static and dynamic disorder. *The Journal of Chemical Physics* **2021**, *155* (13), 134305.

[39] Deng, S.; Shi, E.; Yuan, L.; Jin, L.; Dou, L.; Huang, L. Long-range exciton transport and slow annihilation in two-dimensional hybrid perovskites. *Nature Communications* **2020**, *11* (1).

[40] Zhu, T.; Snaider, J. M.; Yuan, L.; Huang, L. Ultrafast dynamic microscopy of carrier and exciton transport. *Annual Review of Physical Chemistry* **2019**, *70* (1), 219–244.